Research Square

Preprints are preliminary reports that have not undergone peer review.
They should not be considered conclusive, used to inform clinical practice,
or referenced by the media as validated information.

Sustainable Textile Waste in Recycled-Aggregate Concrete: Mechanical Performance, Microstructure, and Cradle-to-Gate Environmental Screening

Abdul Rafay Awan Awan

rafayawan680@gmail.com

Ghulam Ishaq Khan Institute of Engineering Sciences and Technology https://orcid.org/0009-0002-5417-1158

Muhammed Ahmed

Ghulam Ishaq Khan Institute of Engineering Sciences and Technology

Muhammad Faisal javed

University of Tabuk https://orcid.org/0000-0001-5478-9324

Maaz Khan

Ghulam Ishaq Khan Institute of Engineering Sciences and Technology

Hisham Abdulaziz

Prince Sattam Bin Abdulaziz University https://orcid.org/0000-0002-3105-6387

Furqan ahmed

UNHCR, Afghanistan, Kabul, Afghanista

Research Article

Keywords: recycled aggregate concrete, textile waste, polyester-elastane, mechanical properties, microstructure, life-cycle assessment

Posted Date: November 9th, 2026

DOI: https://doi.org/10.21203/rs.3.rs-11640719/v1

License: This work is licensed under a Creative Commons Attribution 4.0 International License.
Read Full License

Additional Declarations: The authors declare no competing interests.

Sustainable Textile Waste in Recycled-Aggregate Concrete: Mechanical Performance, Microstructure, and Cradle-to-Gate Environmental Screening

Abdul Rafay Awan[1]; Muhammad Ahmed[1]; Muhammad Faisal Javed[2]; Maaz Khan[1], Hisham Alabduljabbar[3], Furqan Ahmad[4],

[1]Department of Civil Engineering, GIK Institute of Engineering Sciences and Technology, Topi, Khyber Pakhtunkhwa 23640, Pakistan

[2]Department of Civil Engineering, Faculty of Engineering, University of Tabuk, P.O. Box 741, Tabuk 71491, Saudi Arabia

[3]Department of Civil Engineering, College of Engineering in Al-Kharj, Prince Sattam Bin Abdulaziz University, Al-Kharj 11942, Saudi Arabia

[4]UNHCR, Kabul, Afghanistan

Abstract

Textile waste can provide a secondary reinforcement resource while recycled coarse aggregate (RCA) reduces demand for virgin aggregate, but their combined effects in concrete remain uncertain. This study evaluates nine mixtures combining 0%, 50%, and 100% RCA replacement with 0%, 1%, and 2% apparent-volume fractions of uncoated 95% polyester–5% elastane knitted waste. Slump, fresh density, 28-day compressive strength, and splitting-tensile strength were examined, with selected powders characterized by SEM, XRD, and EDX. At matched RCA levels, 1% textile increased reported mean compressive strength by 5.7–11.8% and splitting-tensile strength by 3.1–4.9%. Nevertheless, strength in the 1% series fell from 33.5 to 27.5 MPa as RCA increased. A descriptive decomposition assigned 85.5% of compressive-strength variation to RCA, 9.7% to textile, and 4.8% to non-additivity. Screening impacts were 506.7–541.7 kg CO_2-eq/m³, with cement contributing 88.1–94.2%. The 1% textile level was the best tested condition, but validation is required before structural or whole-life claims.

Keywords: recycled aggregate concrete; textile waste; polyester-elastane; mechanical properties; microstructure; life-cycle assessment

1. Introduction

Construction and demolition waste is a major materials-management challenge, while continued extraction of virgin aggregate imposes environmental and logistical burdens [1,2]. Recycled coarse aggregate (RCA), produced by crushing concrete waste, can divert material from disposal and reduce demand for natural coarse aggregate [3,4]. Its performance nevertheless depends on source-concrete quality, crushing and screening, particle grading, moisture conditioning, and the amount of adhered old mortar.

Adhered mortar generally lowers RCA density and increases absorption relative to natural coarse aggregate (NCA). It also introduces old-mortar/new-paste and aggregate/mortar interfaces that can reduce workability and strength as the RCA fraction increases [4-8]. These effects connect processing directly to performance: crushing governs adhered mortar and grading, while moisture control governs the effective mixing water and fresh-state response.

Fiber reinforcement has been investigated to restrain crack opening in RCA concrete, although the response depends on fiber material, geometry, dosage, dispersion, and the RCA system [9-13]. Bottle-derived PET fibers, steel-waste-PET hybrids, dynamic loading, and notched-beam fracture have already been studied [14-17], and data-driven synthesis has identified nonlinear interactions among fiber and RCA variables [18]. Those systems establish the technical context but do not represent flexible, uncoated knitted polyester-elastane fabric pieces processed by manual cutting and dispersed during conventional mixing.

Textile-waste cementitious research spans mixed fibers used as fine-aggregate replacement, short random fibers, textile reinforcement, blended fabric waste, cotton knitted fabric, and treated cotton/polyester microfibers [19-24]. Reviews consistently show that workability tends to decline, whereas strength and toughness depend on composition, aspect and surface form, dosage, treatment, dispersion, and matrix type [13,25-28]. Consequently, bottle-derived strips,

separated yarns, treated microfibers, layered textiles, and knitted fabric pieces should not be treated as mechanically interchangeable.

Environmental comparisons are equally sensitive to system definition. Jayalath et al. combined mechanical testing with greenhouse-gas assessment for natural-aggregate textile-fiber concrete [19]. Awan et al. modeled the recovery of RCA and processed textile fiber in Pakistan but did not assess complete concrete mixtures or normalize impacts by concrete strength [29]. The present analysis transfers those recovery factors only as transparent foreground proxies and combines them with the actual nine-mixture inventory and ecoinvent background supply chains. The environmental contribution is therefore a mix-level screening of engineering-efficiency trade-offs, not a repetition of the earlier material-processing study.

The specific contribution is a balanced 3 × 3 comparison of uncoated 95% polyester-5% elastane knitted pieces (approximately 20 × 20 mm) across independently varied RCA levels. The objectives were to: (i) quantify changes in slump and fresh density; (ii) compare reported mean 28-day compressive and splitting-tensile strengths; (iii) separate the RCA, textile, and non-additive components of the nine cell means descriptively; (iv) use SEM, XRD, and EDX as limited microstructural context; and (v) compare absolute and strength-normalized cradle-to-gate impacts. The study does not claim statistical significance, a continuous optimum, structural-code compliance, a verified micromechanical mechanism, or a critically reviewed comparative LCA assertion. Table 1 positions the present study against the closest published precedents

1.1 Research significance and mechanistic premise

The mechanistic premise was that moderate textile content could restrain crack opening or improve stress transfer after mixing, whereas excessive flexible fabric area could impair dispersion and compaction; simultaneously, increasing RCA would amplify absorption and interface heterogeneity. The balanced matrix tests whether these process-related effects remain

additive or become non-additive at high replacement. Because intact interfaces and replicate-level uncertainty were not retained, the premise is evaluated through converging fresh-property and mean-strength patterns rather than claimed as a verified mechanism.

Table 1 Positioning of the present study against the closest published precedents

Study	Matrix and reinforcement	Principal scope	Distinction from present study
Peng et al. [15]	RAC; steel + waste-PET discrete fibers	Fresh properties and static strength; response-surface optimization	Hybrid steel–PET system; not knitted textile fabric
Yan et al. [16]	RAC; bottle-derived PET fibers	Dynamic compression at multiple strain rates	Dynamic response; no textile blend or fresh/tensile matrix
Teixeira and Cerqueira [17]	RAC; 1% PET fibers	Notched-beam fracture response	Single fiber level and fracture focus
Jayalath et al. [19]	Natural-aggregate concrete; mixed textile fibers	Mechanical tests and life-cycle GHG assessment	No RCA factor
Awan et al. [29]	Recovered RCA and processed textile fiber	Material-level recovery LCA per tonne or kilogram	No complete concrete mixture or strength normalization
Juradin et al. [22]	Cement screed; cotton knitted-fabric waste	Strength and fracture energy	Fine mortar/screed; cotton rather than polyester–elastane
Pushpakumara et al. [24]	Mortar; GO-treated cotton + polyester fibers	Fresh, strength, thermal, durability, and SEM	Treated microfibers; no coarse aggregate or RCA
Present study	Concrete; RCA + uncoated polyester–elastane knitted pieces	Balanced 3 × 3 fresh-property/strength matrix; powder-based SEM/XRD/EDX; mix-level LCA screening	Independently varies both wastes and reports absolute and strength-normalized impacts

RAC = recycled-aggregate concrete; PET = polyethylene terephthalate; GO = graphene oxide; GHG = greenhouse gas; LCA = life-cycle assessment. The table positions material form and study design; it is not a performance ranking because the matrices, boundaries, and test methods differ.

2. Materials and Methods

2.1 Materials

2.1.1 Cement

Ordinary Portland cement from Cherat Cement Company (Pakistan), reported as conforming to ASTM C150 [30], was used as the sole binder. The reported physical properties are listed in Table 2 [30,31].

Table 2 Reported physical properties of the Portland cement

Property	Value
Specific gravity (g/cm³)	3.15
Blaine fineness (m²/kg)	301
Initial setting time (min)	145
Final setting time (min)	230
28-day compressive strength (MPa)	45.6

2.1.2 Fine and Coarse Aggregates

Natural river sand had a reported fineness modulus of 2.0 and SSD specific gravity of 2.73 [32,33]. The physical properties of all the aggregates are listed in Table 3. NCA and RCA had a nominal maximum size of 19 mm; their physical properties were determined using ASTM C127 and ASTM C29 procedures [34,35]. The RCA was obtained by crushing and screening demolition-concrete waste. The RCA and NCA are shown in Figure 1(a) and (b). Its lower specific gravity, higher absorption, and lower bulk density relative to NCA are consistent with adhered old mortar [5–7].



Fig. 1 Coarse aggregates used in the study: (a) recycled coarse aggregate (RCA); (b) natural coarse aggregate (NCA)

Table 3 Reported physical properties of fine aggregate, NCA, and RCA

Property	Fine aggregate	NCA	RCA
Specific gravity (SSD)	2.73	2.68	2.35
Specific gravity (oven-dry)	2.69	2.68	2.22
Water absorption (%)	1.5	1.0	6.0
Fineness modulus	2.0	7.5	7.9
Moisture content (%)	0.9	0.5	3.4
Bulk density (kg/m³)	1530	1568	1353

2.1.3 Polyester–Elastane Textile Waste

Knitted textile waste was obtained from a textile facility in Faisalabad, Pakistan. The project record identifies the material as 95% polyester and 5% elastane but does not establish prior consumer use; it is therefore described as manufacturing textile waste rather than post-consumer waste. Before batching, the fabric was manually cut into pieces of approximately 20 × 20 mm. The as received fabric and the cut pieces used in concrete are shown in Figure 2(a) and (b). These were flexible knitted fabric pieces, not monofilament fibers. Table 4 lists the available properties of the fabric. The reported value of 150 kg/m³ is the apparent bulk density used for mixture-volume calculations, not the intrinsic density of the polymer filaments.

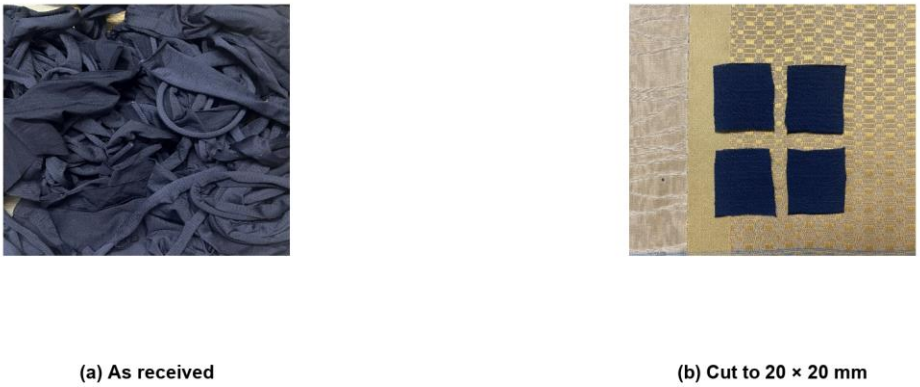


Fig. 2 Polyester–elastane textile waste: (a) knitted fabric as received; (b) fabric cut to approximately 20 × 20 mm for batching

Table 4 Reported properties of the polyester–elastane textile-waste fabric

Composition	Apparent fabric density (kg/m³)	Breaking load, warp (N)	Breaking load, weft (N)	Melting point (°C)	Water response
95% polyester; 5% elastane	150	0.55	0.45	240	Hydrophobic

The breaking-load values are retained for traceability, but the textile test standard, specimen width, and gauge length were unavailable. They are therefore not used to quantify reinforcement efficiency.

2.1.4 Water and Chemical Admixture

Tap water was used for mixing. A polycarboxylate-ether superplasticizer was added at 2.5 kg/m³ in every mixture [36]. The target water-to-binder ratio was 0.40.

2.2 Mixture Matrix and Proportions

Nine mixtures combined three nominal RCA replacement levels (0%, 50%, and 100%) with three nominal textile apparent-volume fractions (0%, 1%, and 2%) using the project mixture-design basis [37]. RCA replacement was calculated on an absolute coarse-aggregate-volume basis. Because RCA and NCA had different specific gravities, the masses at the nominal 50%

level were not equal: 555 kg/m³ NCA and 490 kg/m³ RCA correspond to approximately 49.8% and 50.2% of the combined coarse-aggregate absolute volume, respectively. The textile contents were calculated using the reported apparent fabric density of 150 kg/m³; thus 1.5 and 3.0 kg/m³ correspond to nominal apparent volumes of 1% and 2%. These percentages should not be interpreted as solid-polymer volume fractions.

The 1% and 2% levels were selected to bracket the 1.5% level reported by Jayalath et al. [19], not to establish a continuous optimum. Sand volume was reduced as the nominal textile apparent volume increased. The design free-water content was 205 kg/m³. Moisture and absorption corrections were reportedly applied during batching to achieve SSD-equivalent effective-water conditions. Table 5 therefore reports the mix's proportions and free-water content, not the unrecorded correction water.

Table 5 Design mixture proportions (kg/m³)

Mix	RCA (%)	Textile (%)	Cement	NCA	RCA	Sand	Water	PCE	Textile
M1	0	0	512.5	1110	0	516.6	205	2.5	0
M2	0	1	512.5	1110	0	489.3	205	2.5	1.5
M3	0	2	512.5	1110	0	462.0	205	2.5	3.0
M4	50	0	512.5	555	490	516.6	205	2.5	0
M5	50	1	512.5	555	490	489.3	205	2.5	1.5
M6	50	2	512.5	555	490	462.0	205	2.5	3.0
M7	100	0	512.5	0	980	516.6	205	2.5	0
M8	100	1	512.5	0	980	489.3	205	2.5	1.5
M9	100	2	512.5	0	980	462.0	205	2.5	3.0

RCA replacement is nominal absolute-volume replacement of NCA. Textile percentage is nominal apparent fabric volume based on 150 kg/m³. Water is the design free-water content.

2.3 Processing, Casting, and Curing

Aggregates and sand were dry-mixed for 1 min. Textile pieces were introduced gradually while the mixer operated, after which cement was added and dry mixing continued for 2 min.

The PCE was pre-dissolved in the mixing water and added over approximately 30 s, followed by 2–3 min of wet mixing. Concrete was placed in 150 × 300 mm cylindrical molds in two layers and consolidated on a vibrating table using the same laboratory procedure for every mixture [38]. Specimens were demolded after 24 h and water-cured at 20 ± 2 °C until testing at 28 days. The fixed addition sequence and common consolidation procedure were used to limit processing variation between mixtures; nevertheless, fabric dispersion and entrapped air were not measured.

2.4 Test Methods and Data Treatment

2.4.1 Fresh Properties

Slump was measured within 5 min of mixing in accordance with ASTM C143 [39]. Fresh density was measured using a container of known volume following ASTM C138 [40].

2.4.2 Mechanical Properties

Compressive strength was measured on 150 × 300 mm cylinders at 28 days following ASTM C39, using neoprene caps and a reported loading rate of 4 kN/s [41], and splitting-tensile strength was measured at 28 days by diametral loading following ASTM C496 [42]. The compression and splitting-tensile test configurations are shown in Figure 3(a) and (b). Three cylinders were tested per mixture for each mechanical property, and only the mean strength values are reported along with the standard deviations. Percentage differences are descriptive comparisons of the reported means.



Fig. 3 Mechanical testing: (a) cylinder compression; (b) splitting-tensile loading configuration

2.4.3 Microstructural Characterization and Interpretive Limits

SEM, XRD, and EDX were conducted on five selected mixtures: M1, M2, M3, M4, and M7. Thus, the microstructural dataset compares textile levels only within the 0% RCA series and RCA levels only for textile-free mixtures; it does not directly characterize M5, M6, M8, or M9. Small fragments were collected from specimens, visible textile filaments were manually removed, and the cementitious material was ground. SEM was performed on gold-coated powder at 10,000× and 15 kV [43]. XRD scans were collected from 5° to 60° 2θ at 0.02° per step using Cu-Kα radiation; phases were assigned with Profex 5.7/BGMN [44]. EDX was performed at 15 kV and 1000× on unpolished powder [45]. Powder preparation destroys in-situ spatial geometry; therefore, SEM cannot quantify interfacial-zone width, intact void structure, or crack bridging, and EDX results are treated as semi-quantitative single-composition observations.

2.5 Descriptive Decomposition of Cell Means

The balanced 3 × 3 matrix was also used to separate the variation among the nine reported cell means into an RCA main component, a textile main component, and a non-additive

interaction component. For outcome y_{ij} at RCA level i and textile level j, μ is the grand mean, $\bar{y}_{i\cdot}$ is the RCA-level marginal mean, and $\bar{y}_{\cdot j}$ is the textile-level marginal mean. The additive terms and cell-level interaction residual were calculated as follows:

$$A_i = \bar{y}_{i\cdot} - \mu; \quad B_j = \bar{y}_{\cdot j} - \mu; \quad I_{ij} = y_{ij} - \bar{y}_{i\cdot} - \bar{y}_{\cdot j} + \mu \qquad (1)$$

With a = b = 3 factor levels, the sums of squares were calculated directly from the cell means:

$$SS_R = b\sum_i A_i^2; \quad SS_T = a\sum_j B_j^2; \quad SS_I = \sum_{i\sum_j I_{ij}^2} \quad ; \quad SS_{tot} = \sum_{i\sum_j (y_{ij}-\mu)^2} \qquad (2)$$

$$Share_k(\%) = \frac{100\ SS_k}{SS_{tot}}, \quad k \in \{RCA, textile, interaction\} \qquad (3)$$

This is an exact descriptive decomposition of the observed cell means. Accordingly, the quantities are not inferential ANOVA effect sizes, and no F-tests, p-values, confidence intervals, or claims of statistical significance are presented. The decomposition is used only to organize the observed between-mixture pattern; it does not validate a predictive model or establish causation.

2.6 Cradle-to-Gate Environmental Screening

The environmental calculation was structured according to the goal-and-scope and inventory principles of ISO 14040 and ISO 14044 [46,47], but it is a screening study rather than an independently reviewed ISO-compliant comparative assertion. The functional unit was 1 m³ of concrete at the batching gate. The boundary included the supply of cement, natural coarse aggregate, sand, tap water, and PCE and the recovery-stage processing of RCA and textile waste. Batching electricity, casting, curing, construction, use, maintenance, demolition, and end-of-life processes were excluded because primary data were unavailable or the operations were unchanged among mixtures. The model assigned no credits for avoided landfill disposal, displaced virgin production, carbonation, or extended service life.

Background inventories were calculated in openLCA 2.6.2 [48] using the supplied ecoinvent 3.9.1 cut-off unit-process database [49]. Indian market processes were selected as the closest available regional proxies for Portland cement, crushed gravel, sand, and tap water; a Rest-of-World market for polycarboxylates at 40% active substance was used for the 2.5 kg/m³ admixture because the commercial product solids content was not recorded. Default provider links and market transport embedded in those datasets were retained. The ecoinvent IPCC 2021 method with a 100-year horizon was used to characterize climate-change impacts. The selected central GWP100 category excluded short-lived climate forcers. Total cumulative energy demand (CED) was quantified using the higher-heating-value ecoinvent CED category.

Under cut-off allocation, burdens from the previous product systems were not transferred to the waste inputs. The baseline RCA recovery factors, 0.00886 kg CO_2-eq/kg and 0.1004 MJ-eq/kg, and textile preparation factors, 0.212 kg CO_2-eq/kg and 2.56 MJ-eq/kg, were taken from the authors' earlier Pakistan-specific material-level model [29]. Transferability is imperfect. That RCA model represents industrial recovery of laboratory concrete cylinders with a 70 km transport assumption, whereas the present RCA came from demolition concrete. The earlier textile system represents transported, washed, dried, shredded, opened, and packed loose fiber, whereas the present manufacturing waste was manually cut into fabric pieces. The textile factor is therefore used as a conservative preparation-and-transport proxy, not as a directly measured inventory for the present fabric.

For mixture j, the modeled indicators were calculated by multiplying the design quantity m_{ij} of material i by its unit factor and summing across the seven constituents:

$$GWP_j = \sum_i m_{ij} g_i ; \quad CED_j = \sum_i m_{ij} e_i \qquad (4)$$

For performance normalization, each absolute impact was divided by the reported mean 28-day compressive strength $f_{c,j}$:

$$CI_{GWP,j} = \frac{GWP_j}{f_{c,j}}; \quad CI_{CED,j} = \frac{CED_j}{f_{c,j}} \qquad (5)$$

These intensity ratios compare impact per reported MPa within this dataset; they are not structural functional units and do not account for member design or service life. A deterministic sensitivity bracket varied the cement factors by ±20%, the RCA transport distance from 35 to 140 km using the stage-resolved model in [29], and the textile proxy between preparation-only and preparation-plus-400-km transport. The bracket tests ranking stability but is not a probabilistic uncertainty analysis.

3. Results and Discussion

The results are interpreted through a processing-structure-property framework. Slump and fresh density indicate the combined influence of RCA absorption, fabric volume, and compactability; strength contrasts describe the resulting material response; and powder-based SEM, XRD, and EDX provide only supporting materials context. This hierarchy avoids treating qualitative powder observations as direct proof of the mechanical mechanism.

3.1 Slump

The results of the slump tests on all the mix proportions are presented in Figure 4. Slump decreased as either nominal RCA replacement or textile content increased. In the textile-free series, slump fell from 175 mm (M1) to 132.5 mm (M4) and 95 mm (M7), decreases of 24.3% and 45.7% relative to M1. Within the 0% RCA series, the values were 175, 162.5, and 157.5 mm at 0%, 1%, and 2% textile, respectively. M9 had the lowest reported slump, 75 mm, which was 57.1% below M1.

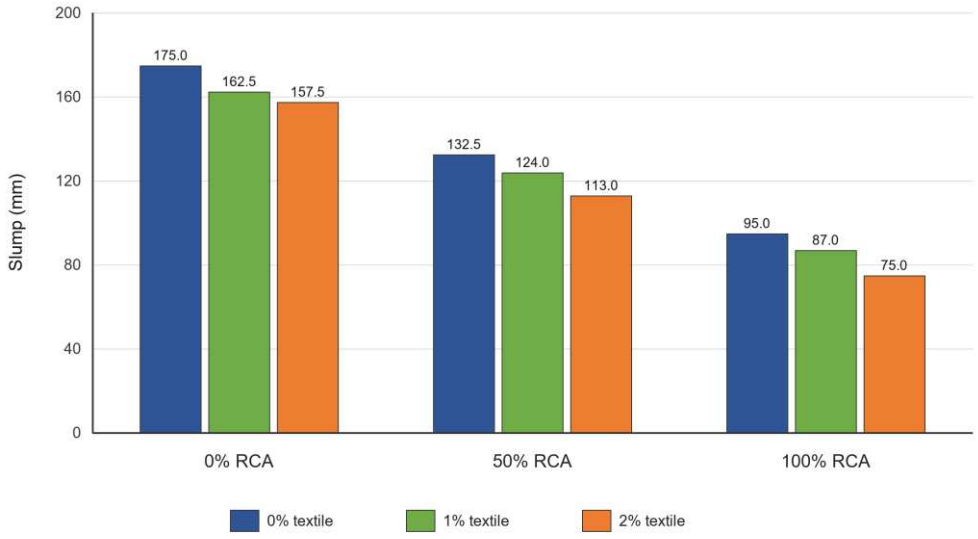


Fig. 4 Reported slump of the nine mixtures.

The trend is consistent with the higher absorption of RCA and the loss of flow commonly observed when dispersed PET or textile reinforcement is added [3,5,15,19,23–25,28,50]. However, batch-specific water corrections and dispersion measurements were unavailable, so those mechanisms were not isolated experimentally. All values were at least 75 mm, and each mixture was consolidated under the stated laboratory procedure. Neither observation by itself demonstrates pumpability, field placement performance, or compliance with a universal workability threshold.

3.2 Fresh Density

Figure 5 shows the results of the Fresh density test. It decreased from 2371 kg/m³ in M1 to 2225 kg/m³ in M9, a difference of 6.2%. In the textile-free series, densities were 2371, 2329, and 2291 kg/m³ at 0%, 50%, and 100% RCA. This ordering is consistent with the lower bulk density and greater porosity of RCA relative to NCA [5,6]. At each RCA level, density also decreased as textile dosage increased, consistent with replacement of part of the sand volume by low-apparent-density fabric.

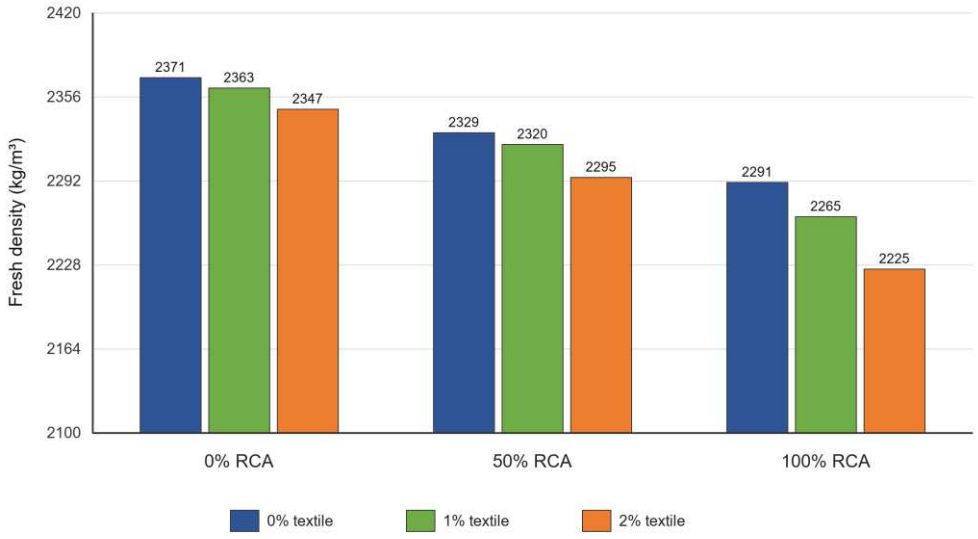


Fig. 5 Reported fresh density of the nine mixtures.

3.3 Compressive Strength

Figure 6 illustrates the compressive strength results. The reported mean 28-day compressive strength of the textile-free series decreased from 31.7 MPa for M1 to 28.1 MPa for M4 and 24.6 MPa for M7, differences of −11.4% and −22.4% relative to M1 shown in Table 6 . This trend is consistent with the effects of adhered mortar and heterogeneous interfaces commonly reported for RCA concrete [3–8].

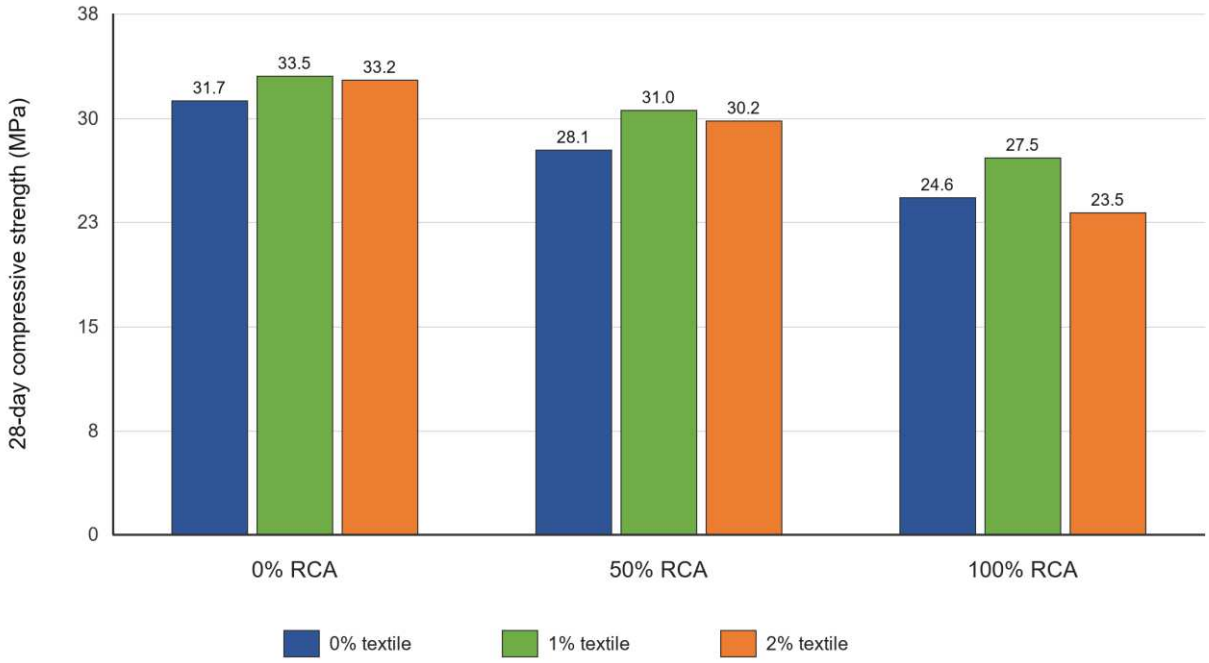


Fig. 6 Reported mean 28-day compressive strength .

At matched RCA levels, the 1% textile mixtures were 5.7% (M2), 10.3% (M5), and 11.8% (M8) above their textile-free controls. The corresponding 2% differences were 4.7% (M3), 7.5% (M6), and −4.5% (M9). These percentages describe within-RCA contrasts; they are not the percentage of RCA-induced strength loss recovered. Importantly, absolute strength across the 1% textile series decreased from 33.5 MPa at 0% RCA to 31.0 MPa at 50% RCA and 27.5 MPa at 100% RCA. Thus, textile addition did not eliminate the absolute RCA-related reduction.

M9 combined the lowest slump with compressive strength below its RCA-matched control. A workability or dispersion effect is plausible and consistent with fiber-reinforced RCA and textile-cementitious literature [9,11,15,23,28], but the present study did not measure fabric distribution, entrapped air, or fracture-surface morphology in M9. The available data therefore identify 1% as the best-performing tested textile level, not as a statistically established optimum or universal upper limit. The mixtures also cannot be assigned structural strength classes or

used to establish code conformity without a specified-strength framework, variability data, and conformity assessment [51].

3.4 Splitting-Tensile Strength

Figure 7 illustrates the splitting-tensile strength results. The textile-free splitting-tensile means decreased from 3.25 MPa (M1) to 2.96 MPa (M4) and 2.67 MPa (M7), differences of −8.9% and −17.8% relative to M1 shown in Table 6. These observations agree qualitatively with reported reductions in RCA concrete [3,5].

At 1% textile, the within-RCA differences were +3.1% for M2, +4.7% for M5, and +4.9% for M8. At 2% textile, the corresponding differences were 0.0%, +1.7%, and −1.9%. M9 was the only textile-containing mixture with values below those of its RCA-matched control in both mechanical tests. The ratios of splitting-tensile to compressive strength ranged from 9.8% to 11.1%, which is within the commonly reported range for normal-strength concrete [52].

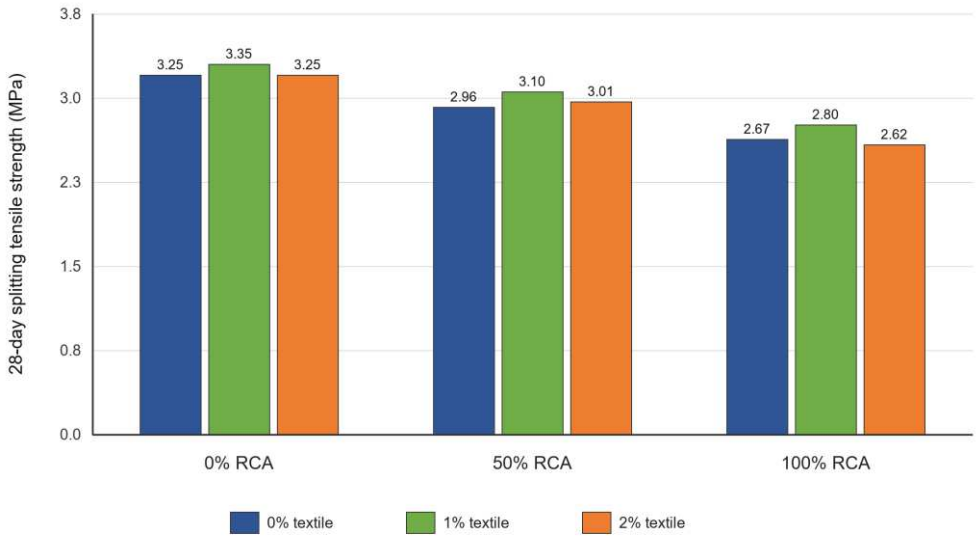


Fig. 7 Reported mean 28-day splitting-tensile strength.

Table 6 Reported 28-day strength means and descriptive percentage differences

Mix	Compressive (MPa)	vs M1 (%)	vs RCA-matched control (%)	Splitting tensile (MPa)	vs M1 (%)	vs RCA-matched control (%)
M1	31.7 ± 1.4	—	—	3.25 ± 0.13	—	—

Mix	Compressive (MPa)	vs M1 (%)	vs RCA-matched control (%)	Splitting tensile (MPa)	vs M1 (%)	vs RCA-matched control (%)
M2	33.5 ± 0.8	+5.7	+5.7	3.35 ± 0.14	+3.1	+3.1
M3	33.2 ± 1.7	+4.7	+4.7	3.25 ± 0.08	0.0	0.0
M4	28.1 ± 1.6	−11.4	—	2.96 ± 0.06	−8.9	—
M5	31.0 ± 2.5	−2.2	+10.3	3.10 ± 0.12	−4.6	+4.7
M6	30.2 ± 1.6	−4.7	+7.5	3.01 ± 0.08	−7.4	+1.7
M7	24.6 ± 1.6	−22.4	—	2.67 ± 0.09	−17.8	—
M8	27.5 ± 1.2	−13.3	+11.8	2.80 ± 0.13	−13.8	+4.9
M9	23.5 ± 1.4	−25.9	−4.5	2.62 ± 0.07	−19.4	−1.9

The RCA-matched controls are M1 for M2–M3, M4 for M5–M6, and M7 for M8–M9. Dashes indicate control rows. Percentages compare reported mean.

3.5 Descriptive Factor and Interaction Effects

The cell-mean decomposition in Table 7 summarizes the observed between-mixture pattern for all four outcomes. The RCA-associated component represented 94.4% of the slump variation, 82.8% of the fresh-density variation, 85.5% of the compressive-strength variation, and 93.8% of the splitting-tensile variation. The textile-associated component represented 5.4%, 14.5%, 9.7%, and 5.5%, respectively. Thus, the textile response is visible in the matched contrasts, but it is smaller than the systematic shift associated with RCA across the tested matrix.

Table 7 Exact descriptive decomposition of observed variation among the nine cell means

Outcome	RCA share (%)	Textile share (%)	Interaction share (%)	Largest absolute interaction residual
Slump	94.4	5.4	0.1	2.39 mm (M2)
Fresh density	82.8	14.5	2.7	12.56 kg/m³ (M9)
Compressive strength	85.5	9.7	4.8	−1.41 MPa (M9)
Splitting-tensile strength	93.8	5.5	0.6	−0.036 MPa (M9)

Shares are based on Eqs. (1)–(3) and may not sum to exactly 100.0% after rounding. Interaction residual = observed cell mean minus the additive prediction from the two marginal means. No residual-error term, F-test, p-value, or confidence interval is available.

The interaction share was small for slump and splitting-tensile strength, but it reached 4.8% for compressive strength. M9 had the largest negative compressive interaction residual (−1.41 MPa), whereas M8 had a positive residual (+0.89 MPa). In practical terms, the 2% textile response at 100% RCA was less favorable than the additive prediction from the two marginal means, whereas the 1% response at 100% RCA was more favorable. Among the three discrete textile levels, this pattern identifies 1% as the best-performing tested level; it does not establish an optimum beyond the tested points or a statistically significant interaction.

3.6 Scanning Electron Microscopy

Figure 8(a)–(e) present SEM micrographs of crushed and coated powder from M1, M2, M3, M4, and M7. Figure 8(a)–(c) show broadly similar rough agglomerates of hydration products, although the displayed M3 field appears locally more open. The M4 and M7 fields (Figure 8(d) and (e)) contain more irregular particles and heterogeneous textures. Such features are compatible with variable quantities of old adhered mortar in RCA mixtures [5,6,53,54], but they are not quantitative measurements of intact porosity, interface quality, or matrix continuity.

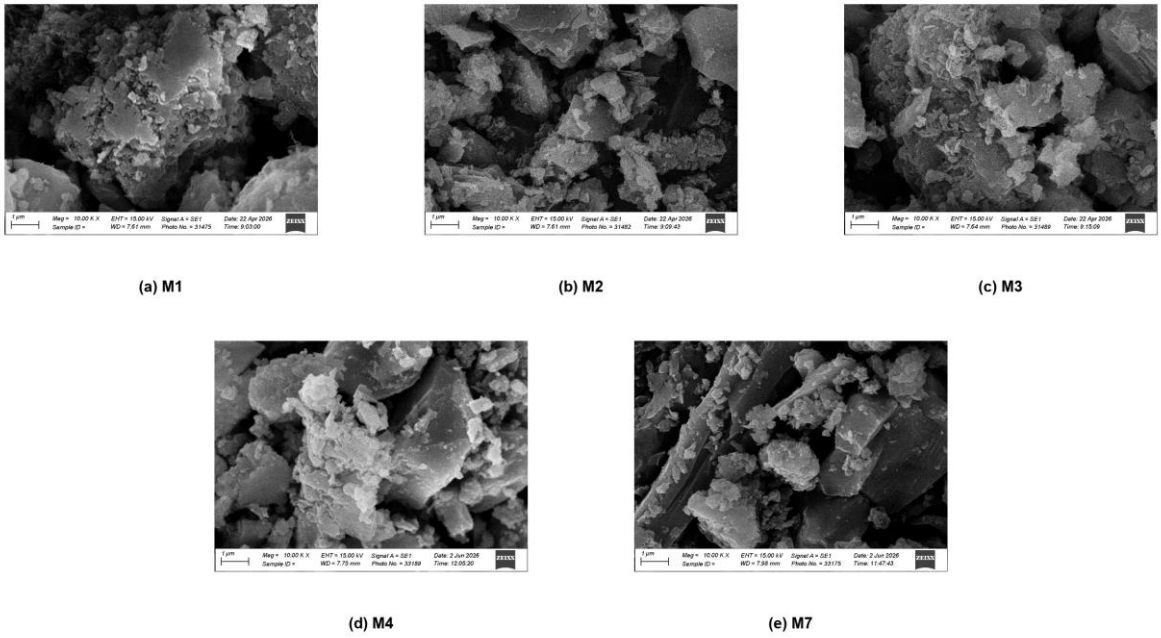


Fig. 8 SEM micrographs of powdered specimens at 10,000×: (a) M1; (b) M2; (c) M3; (d) M4; (e) M7

Because the specimens were powdered and textile filaments were removed, the original aggregate–paste interfaces, crack paths, and fiber–matrix contacts were not preserved. The micrographs therefore cannot confirm crack bridging, measure interfacial transition-zone width, or explain the strength differences causally. They also provide no direct observation of the combined RCA–textile mixtures M5, M6, M8, and M9.

3.7 X-ray Diffraction

The reported XRD patterns and assigned peak positions are shown in Figure 9(a)–(e) and Table 8. Quartz, feldspar, calcite, dolomite, and portlandite were assigned in the dataset, while a reflection near 9.2° 2θ was assigned to ettringite in M4 and M7. Portlandite reflections were reported near 18.1° and 34.1° in M1–M3, near 34.1° in M4, and were not reported for M7.

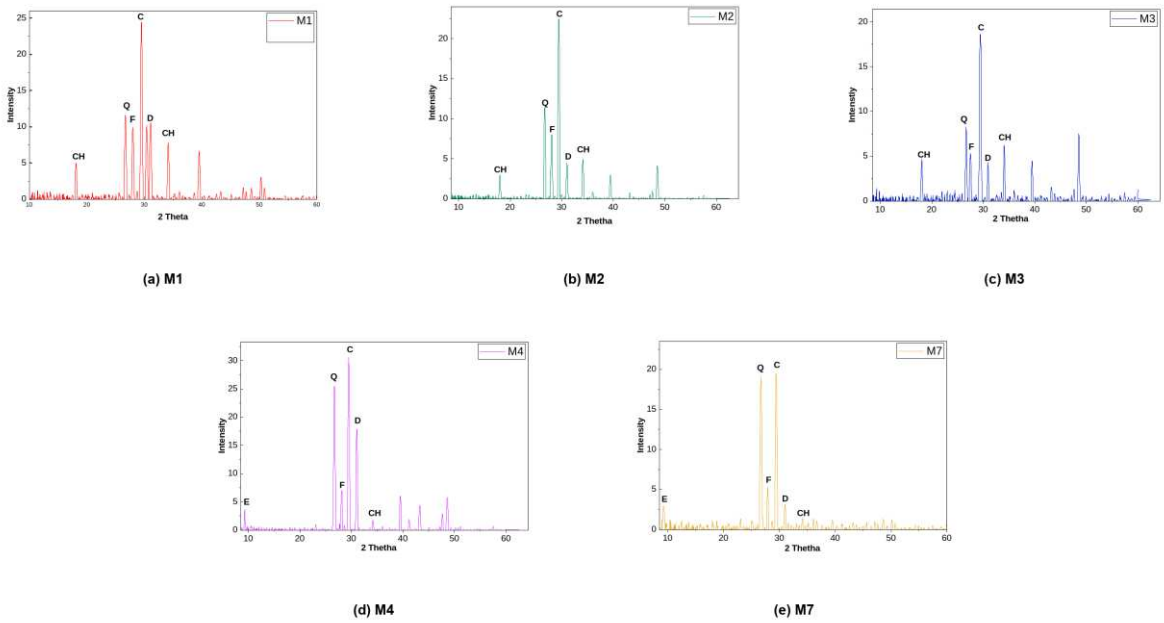


Fig. 9 Reported XRD patterns: (a) M1; (b) M2; (c) M3; (d) M4; (e) M7. Q = quartz, C = calcite, D = dolomite, F = feldspar, CH = portlandite, and E = ettringite

Table 8 Reported crystalline-phase peak positions (2θ, degrees)

Mix	Feldspar	Ettringite	Quartz	Calcite	Dolomite	Portlandite
M1	28.01	—	26.69	29.47	31.04	18.10, 34.16
M2	28.05	—	26.70	29.44	31.04	18.05, 34.12
M3	27.98	—	26.69	29.45	30.95	18.06, 34.14
M4	28.10	9.20	26.69	29.47	31.01	34.15 only
M7	27.90	9.21	26.69	29.42	30.99	—

Because the patterns use different intensity scales and no internal standard, normalization, or Rietveld phase quantification was available, peak heights cannot be compared quantitatively between mixtures. The patterns support qualitative phase identification only; they do not establish calcite enrichment, portlandite suppression, incomplete hydration, or the amount and origin of ettringite [55-59]. The similar assigned phases in M1-M3 provide no evidence that the tested textile levels produced a new crystalline phase.

3.8 Energy-Dispersive X-ray Spectroscopy

Table 9 summarizes the reported EDX composition of M1, M2, M3, M4, and M7, and Figure 10(a)–(e) show the corresponding spectra. Calcium, oxygen, and silicon were the principal detected elements, as expected for cementitious powder. In M1-M3, Ca ranged from 37.91 to 42.74 wt.% and S from 3.72 to 4.16 wt.%; S was 5.54 and 5.80 wt.% in M4 and M7, respectively.

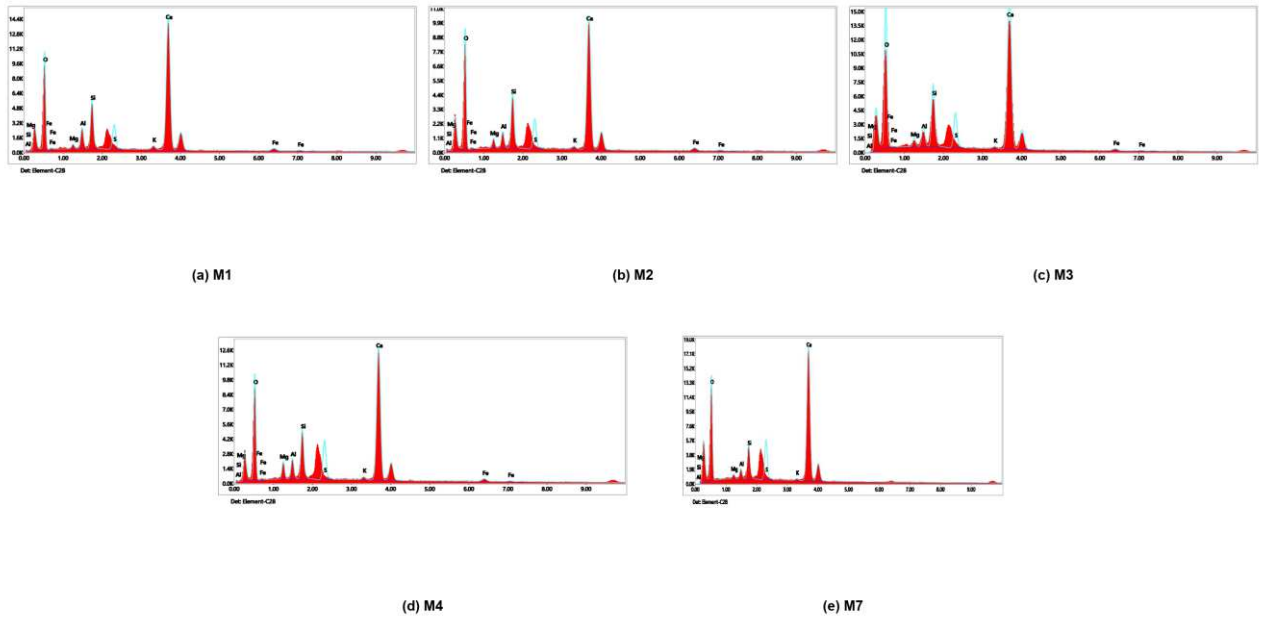


Fig. 10 Reported EDX spectra: (a) M1; (b) M2; (c) M3; (d) M4; (e) M7

Table 9 Reported EDX elemental composition of powdered specimens (wt.%)

Mix	Ca-K	O-K	Si-K	S-K	Al-K	Fe-K	K-K	Mg-K
M1	42.74	41.49	5.57	3.72	2.51	2.53	0.83	0.61
M2	39.44	44.24	5.84	4.16	1.82	2.69	0.61	1.19
M3	37.91	47.54	5.68	4.11	1.91	1.56	0.39	0.90
M4	40.37	40.96	5.39	5.54	2.33	2.62	0.64	2.15
M7	41.90	46.22	3.90	5.80	1.19	—	0.35	0.65

Since the samples were unpolished powder, the observed variations can be attributed to sampling position, sample selection, surface geometry, or true variability [45]. The increased

sulfur values observed in M4 and M7 are consistent with the presence of sulfate minerals or heterogeneity of the old mortar, and the identification of 9.2° from XRD is consistent with this, but it does not provide evidence of sulfate dissolution or secondary ettringite formation.

3.9 Cradle-to-Gate Environmental Screening

Table 10 Unit impact factors used in the screening model

Material	Inventory/proxy and location	GWP100 (kg CO_2-eq/kg)	CED (MJ-eq/kg)
Portland cement	ecoinvent 3.9.1 market, India [49]	0.931171	5.831082
NCA	ecoinvent crushed-gravel market, India [49]	0.038166	0.573384
Sand	ecoinvent sand market, India [49]	0.035923	0.548352
Tap water	ecoinvent tap-water market, India [49]	0.001292	0.016688
PCE	ecoinvent 40%-active market, RoW [49]	1.325853	27.620001
RCA	Pakistan recovery proxy; 70 km [29]	0.008860	0.100400
Textile waste	Pakistan preparation + 400 km proxy [29]	0.212000	2.560000

All reference units are kilograms. NCA = natural coarse aggregate; PCE = polycarboxylate ether; RoW = Rest-of-World. The RCA and textile values are cross-study recovery proxies, not measurements from the present material batches.

Table 11 Baseline cradle-to-gate screening results per cubic metre of concrete

Mix	GWP100 (kg CO_2-eq/m^3)	vs M1 (%)	CED (MJ-eq/m^3)	vs M1 (%)	GWP/f□ (kg CO_2-eq·m^{-3}·MPa^{-1})
M1	541.7	—	3981	—	17.09
M2	541.1	-0.1	3970	-0.3	16.15
M3	540.4	-0.2	3958	-0.6	16.28
M4	524.9	-3.1	3712	-6.8	18.68
M5	524.2	-3.2	3700	-7.0	16.91
M6	523.6	-3.4	3689	-7.3	17.34
M7	508.0	-6.2	3443	-13.5	20.65
M8	507.4	-6.3	3431	-13.8	18.45
M9	506.7	-6.5	3420	-14.1	21.56

GWP/f□ divides modeled GWP by the reported mean 28-day compressive strength. Negative percentages indicate lower absolute impact than M1; they do not establish statistical significance or whole-life superiority.

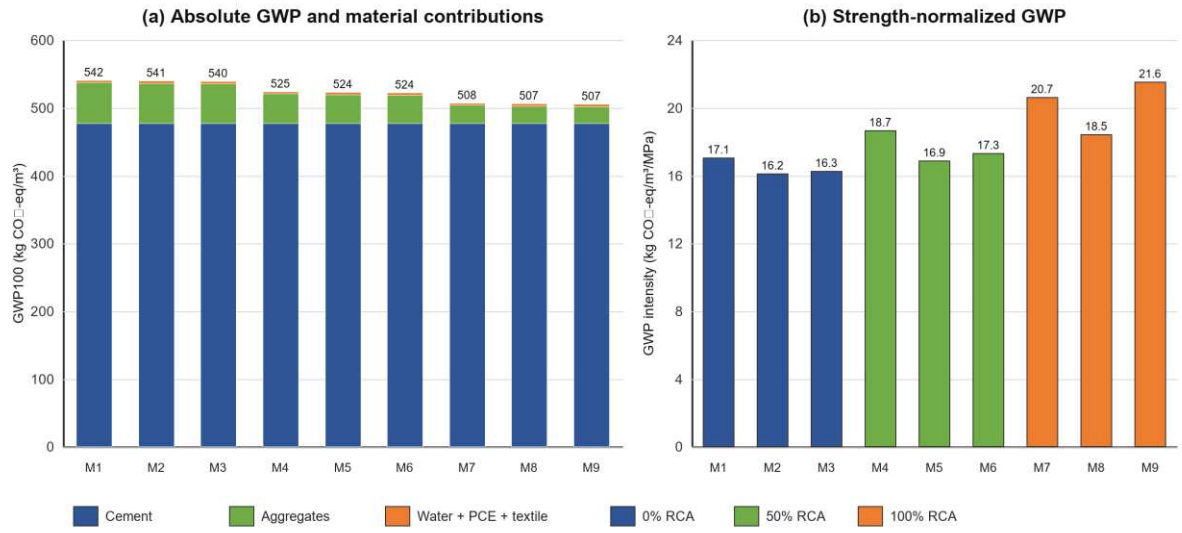


Fig. 11 Baseline cradle-to-gate screening: (a) GWP100 and grouped material contributions; (b) GWP100 normalized by reported mean 28-day compressive strength

The unit impact factors used in the screening model are listed in Table 10. The GWP and CED values across all the mixes are summarized in Table 11. Baseline GWP ranged from 506.7 kg CO_2-eq/m³ (M9) to 541.7 kg CO_2-eq/m³ (M1), while CED ranged from 3420 to 3981 MJ-eq/m³ as illustrated in Figure 11(a) and the strength-normalized GWP is compared in Figure 11(b). Cement contributed 88.1-94.2% of GWP and 75.1-87.4% of CED because every mixture contained 512.5 kg/m³ of cement. Aggregate and textile substitutions therefore changed the modeled totals, but their leverage remained modest relative to the unchanged binder burden.

Within the textile-free series, complete substitution of RCA for NCA reduced modeled GWP and CED by 6.2% and 13.5%, respectively, from M1 to M7. These reductions arise from the specified foreground and background inventories and do not represent avoided-burden credits. Increasing the textile content also slightly reduced absolute modeled impacts because each additional 1.5 kg/m³ of textile coincided with a 27.3 kg/m³ reduction in sand; under the selected factors, the textile-processing burden was smaller than the displaced sand burden.

Absolute impact and mechanical efficiency produced different rankings. M2 had the lowest GWP-to-strength ratio, 16.15 kg CO_2-eq·m^{-3}·MPa^{-1}, which was 5.5% below M1. Although M7

had lower absolute GWP than M1, its ratio was higher (20.65 versus 17.09) because its compressive strength was lower. M9 combined the lowest absolute GWP with the highest ratio, 21.56, which was 26.2% above M1.

Across the nine mixtures, absolute GWP was 408.3–446.3 kg CO_2-eq/m³ under the combined lower sensitivity bound and 607.4–637.2 kg CO_2-eq/m³ under the combined upper bound. The complete ordering by GWP-to-strength ratio remained M2, M3, M5, M1, M6, M8, M4, M7, and M9 from lowest to highest under both bounds. This stability supports the within-dataset ranking but does not remove the uncertainty caused by regional market proxies, the transfer of earlier recovery inventories, or the omission of durability and service life.

4. Engineering Implications and Limitations

Within the tested matrix, the 1% textile mixtures provide the most defensible candidates for further engineering qualification because they consistently exceeded their RCA-matched textile-free controls in both reported mean strengths. The result is a mixture-screening decision, not a design recommendation: the loss of absolute strength with increasing RCA, the reduction in slump, and the absence of durability and variability data prevent direct structural specification. The practical value of the study is therefore the identification of a processing and dosage window for targeted validation rather than immediate field use.

Experimental limitations include one RCA source, one cement system, one water-to-binder ratio, one curing age, and no documented RCA preconditioning state. Textile content is based on apparent fabric density rather than intrinsic polymer volume. The powder-based microstructural subset also excluded combined RCA-textile mixtures and cannot resolve intact interfaces or causal mechanisms.

The environmental model is attributional and cradle-to-gate. It uses Indian ecoinvent markets as regional proxies, a Rest-of-World PCE proxy, and recovery factors transferred from a prior Pakistan study whose processing routes do not exactly match the present materials.

Supplier-specific cement data, measured transport and cutting energy, batching and curing energy, construction losses, service life, and end-of-life were unavailable. The deterministic sensitivity bounds test ranking stability but do not represent parameter probabilities. The results therefore support transparent screening within this mixture set, not an environmental product declaration or a public comparative assertion.

5. Recommendations for Further Validation

The current results define a focused validation path:

- Examine textile contents around 1% while measuring intrinsic polymer volume, fabric dispersion, entrained air, rheology, and the influence of RCA moisture conditioning.
- Use polished cross-sections, fracture surfaces, repeated EDX mapping, and quantitative XRD to resolve intact aggregate-paste and textile-paste interfaces, then relate them to flexure, fracture, shrinkage, and durability.
- Validate multiple RCA and textile sources and replace the screening LCA proxies with supplier-specific cement, transport, recovery, batching, service-life, and end-of-life inventories before making comparative claims.

6. Conclusions

The following conclusions are limited to the tested materials, mixture levels, and descriptive dataset:

- RCA was the dominant source of the observed response. In textile-free concrete, increasing RCA from 0% to 100% reduced slump by 45.7%, fresh density by 3.4%, compressive strength by 22.4%, and splitting-tensile strength by 17.8% relative to M1.
- At each RCA level, the nominal 1% textile apparent-volume fraction produced the highest reported mean strengths among the three tested textile levels. Its compressive-strength

differences relative to RCA-matched controls were +5.7%, +10.3%, and +11.8% at 0%, 50%, and 100% RCA, respectively.

- The textile contribution did not remove the absolute RCA penalty: compressive strength in the 1% textile series decreased from 33.5 MPa at 0% RCA to 27.5 MPa at 100% RCA. At 100% RCA, increasing textile from 1% to 2% coincided with the lowest slump and lower compressive strength than the textile-free control.
- The exact cell-mean decomposition attributed 85.5% of compressive-strength variation to RCA, 9.7% to textile, and 4.8% to non-additivity. These shares organize the observed means but are not inferential ANOVA effect sizes.
- Powder-based SEM, XRD, and EDX supplied qualitative materials context only. They did not preserve intact aggregate-paste or textile-paste interfaces and therefore cannot verify crack bridging or a causal mechanism.
- Full RCA replacement reduced modeled cradle-to-gate GWP by 6.2% and CED by 13.5% in the textile-free series, but the GWP-to-strength ratio increased. M2 provided the lowest modeled GWP-to-strength ratio, whereas M9 combined the lowest absolute GWP with the highest ratio.
- Accordingly, 1% is the best-performing tested textile level, not a statistically established optimum. The results support mixture screening and prioritization for further qualification; they do not alone establish durability, field constructability, structural-code conformity, or whole-life environmental superiority.

7. Statements and Declarations

7.1 Funding

The authors received no financial support for the research, authorship, or publication of this article.

7.2 Competing Interests

The authors declare no competing interests.

7.3 Data Availability

The processed mixture means and environmental inventories needed to reproduce the reported tables are contained in this article. Derived calculation files are available from the authors on reasonable requests.

References

[1] Patil, S., Gupta, A., & Rathore, V. S. Recycling of construction and demolition waste in the sector of construction. Advances in Civil Engineering, vol. 2024, p. 6234010. https://doi.org/10.1155/2024/6234010

[2] UNEP. Sand and Sustainability: 10 Strategic Recommendations to Avert a Crisis. United Nations Environment Programme, Nairobi, 2022. Available at: https://www.unep.org/resources/report/sand-and-sustainability-10-strategic-recommendations-avert-crisis

[3] Panghal, H., & Kumar, A. Structural aspects of concrete incorporating recycled coarse aggregates from construction and demolished waste. Materiales de Construcción, vol. 74(353), p. e337. https://doi.org/10.3989/mc.2024.360023

[4] Piccinali, A., Diotti, A., Plizzari, G., & Sorlini, S. Impact of recycled aggregate on the mechanical and environmental properties of concrete: a review. Materials, vol. 15(5), p. 1818. https://doi.org/10.3390/ma15051818

[5] Etxeberria, M., Vázquez, E., Marí, A., & Barra, M. Influence of amount of recycled coarse aggregates and production process on properties of recycled aggregate concrete. Cement and Concrete Research, vol. 37(5), p. 735–742. https://doi.org/10.1016/j.cemconres.2007.02.002

[6] Abubakr S, Lomboy GR, & Cleary DB. Recycled Concrete Aggregates: Production, Properties of RCA and RCA-Based Concrete, and Economic Considerations. Recent Progress in Materials, vol. 8(2), p. 004, 2026. https://doi.org/10.21926/rpm.2602004

[7] Tam, V. W. Y., Tam, C. M., & Le, K. N. Removal of cement mortar remains from recycled aggregate using pre-soaking approaches. Resources, Conservation and Recycling, vol. 50(1), p. 82–101. https://doi.org/10.1016/j.resconrec.2006.05.012

[8] Poon, C. S., Shui, Z. H., & Lam, L. Effect of microstructure of ITZ on compressive strength of concrete prepared with recycled aggregates. Construction and Building Materials, vol. 18(6), p. 461–468. https://doi.org/10.1016/j.conbuildmat.2004.03.005

[9] Yao, X., Pei, Z., Zheng, H., Guan, Q., Wang, F., Wang, S., & Ji, Y. Review of mechanical and temperature properties of fiber reinforced recycled aggregate concrete. Buildings, vol. 12(8), p. 1224. https://doi.org/10.3390/buildings12081224

[10] Zhang, L., Li, X., Li, C., Zhao, J., & Cheng, S. Mechanical properties of fully recycled aggregate concrete reinforced with steel fiber and polypropylene fiber. Materials, vol. 17(5), p. 1156. https://doi.org/10.3390/ma17051156

[11] Liu, Z., Chen, Y., et al. Experimental study on mechanical properties of recycled aggregate concrete with polypropylene fiber under combined compression–shear loading. Structural Concrete, vol. 25(2), p. 810–825. https://doi.org/10.1002/suco.202300088

[12] Pham, T. M. Fibre-reinforced concrete: state-of-the-art review on bridging mechanism, mechanical properties, durability, and eco-economic analysis. Case Studies in Construction Materials, vol. 22, p. e03893. https://doi.org/10.1016/j.cscm.2024.e03893

[13] Fode, T. A., Jande, Y. A. C., & Kivevele, T. Physical, mechanical, and durability properties of concrete containing different waste synthetic fibers for green environment—A critical review. Heliyon, 10, e32950 (2024). https://doi.org/10.1016/j.heliyon.2024.e32950

[14] Pelisser, F., Montedo, O. R. K., Gleize, P. J. P., & Roman, H. Mechanical properties of recycled PET fibres in concrete. Chemical Engineering Journal, vol. 173(2), p. 190–196. https://doi.org/10.1016/j.cej.2011.07.046

[15] Peng, Q., Chen, B., Lu, Q., Li, K., & Jin, W. Effect of steel-waste PET hybrid fiber on properties of recycled aggregate concrete based on response surface methodology. Construction and Building Materials, 397, 132448 (2023). https://doi.org/10.1016/j.conbuildmat.2023.132448

[16] Yan, Z.-W., Bai, Y.-L., & Chen, W. Dynamic compressive behaviors of polyethylene terephthalate fiber reinforced recycled aggregate concrete. Structural Concrete, 25, 3883–3901 (2024). https://doi.org/10.1002/suco.202300756

[17] Teixeira, A. C. M., & Cerqueira, N. A. Influence of 1% recycled PET fiber on the fracture behavior of recycled aggregate concrete beams. Revista Matéria, 31 (2026). https://doi.org/10.1590/1517-7076-RMAT-2025-0961

[18] Arifuzzaman, M., & Gazder, U. Unraveling the synergistic effects of fibers and recycled aggregates in concrete using ensemble machine-learning approach. Journal of Structural Design and Construction Practice, 31(4), 04026083 (2026). https://doi.org/10.1061/JSDCCC.SCENG-2203

[19] Jayalath, A., Sofi, M., Ginigaddara, T., Gou, H., Mendis, P., & Aye, L. Mechanical properties and life cycle greenhouse gas analysis of textile waste fibre-based concrete. Construction and Building Materials, 428, 136267 (2024). https://doi.org/10.1016/j.conbuildmat.2024.136267

[20] Sadrolodabaee, P., Claramunt, J., Ardanuy, M., & de la Fuente, A. A textile waste fiber-reinforced cement composite: comparison between short random fiber and textile reinforcement. Materials, vol. 14(13), p. 3742. https://doi.org/10.3390/ma14133742

[21] Tran, N. P., Gunasekara, C., Law, D. W., Houshyar, S., & Setunge, S. Repurposing of blended fabric waste for sustainable cement-based composite: mechanical and microstructural performance. Construction and Building Materials, vol. 362, p. 129785. https://doi.org/10.1016/j.conbuildmat.2022.129785

[22] Juradin, S., Bartulović, B., Žižić, D., & Mrakovčić, S. Cotton knitted fabric waste as reinforcement in cement screed. Advances in Civil and Architectural Engineering, 15(28), 1–14 (2024). https://doi.org/10.13167/2024.28.1

[23] Janta, P., Koottatep, T., Xue, W., Anwar, N., & Polprasert, C. Effects of micro- and macro-fibers in Textile Cementitious Composite (TCC) on mechanical performance and their green alternative approaches. Journal of Sustainable Cement-Based Materials, 15(9), 2981–2996 (2026). https://doi.org/10.1080/21650373.2026.2669216

[24] Pushpakumara, B. H. J., Subawickrama, S. G. D. L., De Silva, G. H. M. J. S., Samarakoon, S. M. S. M. K., & Gebremariam, K. F. Effect of graphene oxide-treated textile waste cotton and polyester fibers on fresh, mechanical, thermal and durability properties of cement mortar. Construction and Building Materials, 527, 146432 (2026). https://doi.org/10.1016/j.conbuildmat.2026.146432

[25] Tran, N. P., Gunasekara, C., Law, D. W., Houshyar, S., Setunge, S., & Cwirzen, A. Comprehensive review on sustainable fiber-reinforced concrete incorporating recycled textile waste. Journal of Sustainable Cement-Based Materials, 11(1), 28–42. https://doi.org/10.1080/21650373.2021.1875273

[26] Shahriar, M. F., Rahman, R., & Kamal, T. An overview of the application of recycled textile fibers in structural concrete. Discover Concrete and Cement, 1, Article 29 (2025). https://doi.org/10.1007/s44416-025-00029-1

[27] Sasi, S., Kumar, P. K., & Mathai, A. A review on the effects of waste textile polymer fiber on concrete strength: exploring the key parameters. Buildings, vol. 14(5), p. 1486. https://doi.org/10.3390/buildings14051486

[28] Incerti, A. T., Bruschi, G. J., & Korf, E. P. Textile waste reinforced cementitious composites: state of the art and future perspectives. Environmental Science and Pollution Research, 33, 12642–12658 (2026). https://doi.org/10.1007/s11356-026-38099-8

[29] Awan, A. R., Saif, M. H., & Javed, M. F. Environmental life cycle assessment of recycled coarse aggregate and textile waste fibers. Fusion Journal of Engineering and Sciences, Special Issue CCETC-2026 (2026). https://doi.org/10.64615/fjes.2026.145

[30] ASTM C150/C150M-22. Standard Specification for Portland Cement. ASTM International, West Conshohocken, PA, 2022. https://doi.org/10.1520/C0150_C0150M-22

[31] Bilal, H., Alam, M., Khattak, N. U., Yasir, M., Suliman, M., & Ali, K. Physical Properties of Different Brands of Cement Manufactured in KPK, Pakistan: A Case Study. Pakistan Journal of Engineering and Technology (PakJET), vol. 5(4), p. 63--67, 2022. https://doi.org/10.51846/vol5iss4pp63-67

[32] ASTM C136/C136M-19. Standard Test Method for Sieve Analysis of Fine and Coarse Aggregates. ASTM International, West Conshohocken, PA, 2019. https://doi.org/10.1520/C0136_C0136M-19

[33] ASTM C128-22. Standard Test Method for Relative Density (Specific Gravity) and Absorption of Fine Aggregate. ASTM International, West Conshohocken, PA, 2022. https://doi.org/10.1520/C0128-22

[34] ASTM C127-15. Standard Test Method for Relative Density (Specific Gravity) and Absorption of Coarse Aggregate. ASTM International, West Conshohocken, PA, 2015. https://doi.org/10.1520/C0127-15

[35] ASTM C29/C29M-17a. Standard Test Method for Bulk Density (Unit Weight) and Voids in Aggregate. ASTM International, West Conshohocken, PA, 2017. https://doi.org/10.1520/C0029_C0029M-17A

[36] ACI Committee 212. ACI 212.3R-16: Report on Chemical Admixtures for Concrete. American Concrete Institute, Farmington Hills, MI, 2016.

[37] ACI 211.1-91. Standard Practice for Selecting Proportions for Normal, Heavyweight, and Mass Concrete. ACI International, Farmington Hills, MI, 2002.

[38] ACI Committee 309. Guide for Consolidation of Concrete. ACI 309R-05. American Concrete Institute, Farmington Hills, MI, 2005.

[39] ASTM C143/C143M-20. Standard Test Method for Slump of Hydraulic-Cement Concrete. ASTM International, West Conshohocken, PA, 2020. https://doi.org/10.1520/C0143_C0143M-20

[40] ASTM C138/C138M-17a. Standard Test Method for Density (Unit Weight), Yield, and Air Content (Gravimetric) of Concrete. ASTM International, West Conshohocken, PA, 2017. https://doi.org/10.1520/C0138_C0138M-17A

[41] ASTM C39/C39M-21. Standard Test Method for Compressive Strength of Cylindrical Concrete Specimens. ASTM International, West Conshohocken, PA, 2021. https://doi.org/10.1520/C0039_C0039M-21

[42] ASTM C496/C496M-17. Standard Test Method for Splitting Tensile Strength of Cylindrical Concrete Specimens. ASTM International, West Conshohocken, PA, 2017. https://doi.org/10.1520/C0496_C0496M-17

[43] Scrivener, K. L., Bazzoni, A., Mota Gassó, B., & Rossen, J. E. Electron microscopy. In: K. L. Scrivener, R. Snellings, & B. Lothenbach (Eds.), A Practical Guide to Microstructural Analysis of Cementitious Materials (pp. 107–161). CRC Press, Boca Raton, FL, 2016

[44] Scrivener, K. L., Snellings, R., & Lothenbach, B. (Eds.). A Practical Guide to Microstructural Analysis of Cementitious Materials. CRC Press, Boca Raton, FL, 2016

[45] Snellings, R., Baken, S., Janssen, A., Van den Heede, P., Cizer, K., & Elsen, J. Optimization of SEM-EDS to determine the C–A–S–H composition in matured cement paste samples. Materials Characterisation, vol. 123, p. 10–19. https://doi.org/10.1016/j.matchar.2016.11.021

[46] International Organization for Standardization. ISO 14040:2006, Environmental management—Life cycle assessment—Principles and framework, with Amendment 1:2020. Geneva: ISO.

[47] International Organization for Standardization. ISO 14044:2006, Environmental management—Life cycle assessment—Requirements and guidelines, with Amendments 1:2017 and 2:2020. Geneva: ISO.

[48] GreenDelta GmbH. openLCA, version 2.6.2. Berlin, Germany (2026). https://www.openlca.org/

[49] Wernet, G., Bauer, C., Steubing, B., Reinhard, J., Moreno-Ruiz, E., & Weidema, B. The ecoinvent database version 3 (part I): overview and methodology. International Journal of Life Cycle Assessment, 21, 1218–1230 (2016). https://doi.org/10.1007/s11367-016-1087-8

[50] Thomas, J., Thaickavil, N. N., & Wilson, P. M. Strength and durability of concrete containing recycled concrete aggregates. Journal of Building Engineering, vol. 19, p. 349–365, 2018. https://doi.org/10.1016/j.jobe.2018.05.007

[51] EN 206:2013+A2:2021. Concrete — Specification, Performance, Production and Conformity. European Committee for Standardization, Brussels, 2021.

[52] Neville, A. M. Properties of Concrete, 5th ed. Pearson Education, Harlow, England, 2011.

[53] Richardson, I. G. The calcium silicate hydrates. Cement and Concrete Research, vol. 38(2), p. 137–158. https://doi.org/10.1016/j.cemconres.2007.11.005

[54] Li, C., Zhang, X., Cao, X., & Yu, Y. Sustainable Performance and Interfacial Characteristics of Fully Recycled Concrete with Combined Recycled Concrete, Brick, and Ceramic Aggregates. Sustainability, vol. 17(23), p. 10503, 2025. https://doi.org/10.3390/su172310503

[55] Angulo, S. C., Ulsen, C., John, V. M., Kahn, H., & Cincotto, M. A. Chemical–mineralogical characterisation of coarse recycled concrete aggregate. Waste Management, vol. 29(2), p. 721–730. https://doi.org/10.1016/j.wasman.2008.06.005

[56] Taylor, H. F. W. Cement Chemistry (2nd ed.). Thomas Telford, London, 1997

[57] Colman, C., Bulteel, D., Thiery, V., Rémond, S., Michel, B., & de Luca Pennec, L. Internal sulfate attack in mortars containing contaminated fine recycled concrete aggregates. Construction and Building Materials, vol. 272, p. 121851. https://doi.org/10.1016/j.conbuildmat.2020.121851

[58] Collepardi, M. A state-of-the-art review on delayed ettringite attack on concrete. Cement and Concrete Composites, vol. 25(4–5), p. 401–407. https://doi.org/10.1016/S0958-9465(02)00080-X

[59] Scrivener, K. L., Juilland, P., & Monteiro, P. J. M. Advances in understanding hydration of Portland cement. Cement and Concrete Research, 78, 38–56. https://doi.org/10.1016/j.cemconres.2015.05.025